Maximization of PV energy use and performance analysis of a stand-alone PV-hydrogen system

Martinez Lopez, V. A.; Ziar, H.; Zeman, M.; Isabella, O.

DOI
10.1016/j.ijhydene.2023.09.072

Publication date
2023

Document Version
Final published version

Published in
International Journal of Hydrogen Energy

Available online at www.sciencedirect.com

ScienceDirect

journal homepage: www.elsevier.com/locate/he

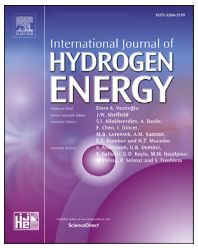

Maximization of PV energy use and performance analysis of a stand-alone PV-hydrogen system

V.A. Martinez Lopez*, H. Ziar, M. Zeman, O. Isabella

Delft University of Technology, Photovoltaic Materials and Devices Group, EEMCS Faculty, Mekelweg 4, Delft, 2628CD, the Netherlands

HIGHLIGHTS

- Optimization of stand-alone hydrogen system fully powered by PV.
- Analysis of the orientation of the PV modules as decision variables.
- Definition of three performance indicators.
- Analysis of operation at partial loads.

ARTICLE INFO

Article history:
Received 9 January 2023
Received in revised form
6 September 2023
Accepted 7 September 2023
Available online 4 October 2023

Keywords:
Stand-alone system
particle swarm optimization
PV-hydrogen system
alkaline electrolyzer

ABSTRACT

The development of clean hydrogen and photovoltaic (PV) systems is lagging behind the goals set in the Net Zero Emissions scenario of the International Energy Agency. For this reason, efficient hydrogen production systems powered from renewable energy need to be deployed faster. This work presents an optimization procedure for a stand-alone, fully PV-powered alkaline electrolysis system. The approach is based on the Particle Swarm Optimization algorithm to obtain the best configuration of the PV plant that powers the electrolyzer and its compressor. The best configuration is determined with one of three indicators: cost, efficiency, or wasted energy. The PV plant needs to be oversized 2.63 times with respect to the electrolyzer to obtain minimum cost, while for high efficiency, this number increases by 2%. Additionally, the configuration that minimizes cost, wasted energy or maximizes efficiency does not correspond to the configuration that maximizes the annual PV yield. Optimizing for cost results also leads to the best operation of the electrolyzer at partial loads than optimizing for efficiency or wasted energy.

1. Introduction

"More efforts needed" is the status of the International Energy Agency tracking report in hydrogen [1]. This means that the deployment of hydrogen with low emissions is still below the expected targets toward the 2050 Net Zero Emissions scenario [1]. Traditional hydrogen generation exceeded 900 Mt_{CO_2} emissions, and only a minority of the total hydrogen produced came from clean sources. While the use of hydrogen diversifies in other sectors beyond refining and chemistry, these two sectors demand more than 90% of the global hydrogen production [1]. Because of the emission-intensive generation

* *Corresponding author.*
E-mail address: V.A.MartinezLopez@tudelft.nl (V.A. Martinez Lopez).
https://doi.org/10.1016/j.ijhydene.2023.09.072

List of symbols

V_{act}	Activation voltage
α	Albedo
T_a	Ambient temperature
A_{module}	Area of the PV module
A_m	Azimuth of the PV module
A_s	Azimuth of the Sun
A	Cell area
V_{cell}	Cell voltage
ΔG	Change of Gibbs free energy
P_{comp}	Compressor power
i	Current density
$P_{curtailed}$	Curtailed power
G_{diff}	Diffuse irradiance
n_d	Diode ideality factor
G_{dir}	Direct irradiance
η	Efficiency
I	Electrolyzer current
P_{min}	Electrolyzer minimum operating power
P_{nom}	Electrolyzer nominal power
P_{ele}	Electrolyzer power
I_{stack}	Electrolyzer stack current
a_s	Elevation of the Sun
H	Enthalpy of hydrogen
F	Faraday's constant
η_F	Farday's efficiency
$\dot{H}_2$	Hydrogen flow
C_p	Hydrogen specific heat at constant pressure
C_v	Hydrogen specific heat at constant volume
I_t	Investment costs
M_t	Maintenance costs
r	Modeling parameter, discount rate
s	Modeling parameter
t	Modeling parameter, time
n	Moles of hydrogen
T_{NOCT}	Nominal Operating Cell Temperature
N_{cells}	Number of electrolyzer cells
G_m	Plane-of-array irradiance
α_p	Power deviation coefficient
P	Pressure
H_t	Produced hydrogen
η	PV module efficiency at Standard Test Conditions
P_{mpp}	PV module maximum power point at Standard Test Conditions
P_{PV}	PV power
γ	Ratio of specific heats
G_{ref}	Reflected irradiance
V_{rev}	Reversible voltage
T	Temperature
T_m	Temperature of the PV module
a_m	Tilt of the PV module
R	Universal gas constant
P_{unused}	Unused power
V_{ele}	Stack voltage
W	Work needed to compress hydrogen

methods and the importance of hydrogen in hard-to-decarbonize sectors, such as transport and industry, hydrogen production from electricity and water (electrolysis) is expected to cover around 75% of the clean hydrogen demand worldwide by 2030.

Solar photovoltaic (PV) energy is becoming a preferred option for powering water electrolyzers for hydrogen production with three methods for interconnecting such systems [2]:

Directly-coupled systems. These systems rely on finding an operating point such that the I–V curves of the PV system and that of the electrolyzer intersect at a point that is close to the maximum power point (MPP) of the PV [2]. Direct-coupling systems can be made more efficient by applying load-management techniques, which consist of dynamically changing the number of electrolyzer stacks connected in parallel using a switch. In this way, a discrete MPP tracker can be implemented reaching coupling efficiencies close to 99% [2]. These systems are also suited for low-power applications (below 1 kW) for their simplicity, safety, and cost [3].

DC-DC coupling. The electrolyzer can also be interfaced with the PV system using a DC-DC converter which decouples the operating point of the PV system from that of the electrolyzer. The PV system can operate at its maximum power point at every instant and does not depend on the component design as with the directly coupled systems [4]. Even when there is one conversion stage that causes power loss, the total efficiency of the system is higher than the static directly coupled system (without load management) mainly because of the deviation from the MPP of the latter at low irradiance [4].

The advantage of using a DC-DC converter is that the performance of the system improves under changing irradiance. A maximum power point tracking algorithm forces the PV modules to deliver, as the name implies, maximum power. However, the algorithm can also drive the electrolyzer into dangerous conditions either above or below the design limits. For this reason, a modified MPP tracking algorithm was proposed in Ref. [5], which allows tracking of the MPP under most conditions, but adjusts the set point if the electrolyzer approaches an unsafe operating point.

AC coupling. This configuration is typically used to connect electrolyzers to grid-connected PV systems. The connection is made using an inverter at the output of the PV system and a rectifier at the input of the electrolyzer. Similar to the DC-DC coupling, the AC coupling systems can perform MPPT [2]. For grid-connected systems, transformers are also needed besides the DC-AC-DC conversion, resulting in 4 power processing stages with associated losses [2]. AC conversion can also be used in off-grid PV-electrolysis systems as in Ref. [6]. This system needs only two conversion stages (one inverter on the PV side and one rectifier on the electrolyzer side).

Direct coupling systems are well suited for small-scale projects, DC coupling for PV systems located in proximity to the electrolyzer, and AC coupling strategy is adequate for large-scale systems (in the MW range) where the PV production plant is far from the electrolyzer [2].

In all interconnection modalities, optimization must be performed to ensure maximum hydrogen production, minimum cost, and maximum efficiency.

1.1. *Optimization of PV-electrolyzer systems*

The sizing of the PV-electrolyzer plant depends on the coupling strategy and is an optimization problem of finding the configuration (in terms of size of PV and EL) that maximizes or minimizes efficiency, hydrogen production, cost, etc.

Directly-coupled systems are typically optimized by choosing an appropriate number of PV modules, electrolyzer cells, or both and the connection between them (series or parallel). To achieve this, a statistical approach can be employed. The basis of this method is to identify the region in the I–V plane where the MPP of a given PV module occurs frequently and obtain the fraction of the maximum power point current at which the energy density is the highest. Then, the number of series connected electrolyzer cells is tuned such that the system operates in the highest energy density region. This method allows the use of readily available manufacturer data and applies to alkaline and PEM technologies [3]. Additionally, the I–V curve of the PV module can be linearized around the MPP. The resultant expression is a linear equation that relates the maximum power point current and voltage. A similar approach is made for the current of the electrolyzer. These expressions are then expanded by including the number of series and parallel PV modules and electrolyzer cells. When the linearized equations of both components are equated, the number of series and parallel modules and cells for a given temperature are obtained. This system will operate with very high coupling efficiencies regardless of the changing irradiance, as long as the operating temperature is kept at the design parameter [7].

Metaheuristic approaches, which are based on stochasticity and the repetitive evaluation of the objective function [8], are also often used to optimize directly-coupled PV systems. The number of series, parallel PV modules, and series, parallel electrolyzer cells is used as a decision variable. The genetic algorithm [9,10], the imperialist competitive algorithm [11], and particle swarm optimization [12,13] have been employed in the past to obtain the best configuration of PV and electrolyzer.

Naturally, an *a posteriori* analysis can also be conducted to study the response of the system to different parameters and find an optimal solution. This is the case for the study of [14] for a combined PV-thermal system. The optimal solution can be found by increasing the number of parallel PV modules and the number of series-connected electrolysis stacks and then analyzing the efficiency.

For DC-DC coupled systems, Gillisen et al. [15], found the optimal size that minimizes the hydrogen cost for a fictitious power-to-gas installation in Germany powered exclusively by a PV system. The number of alkaline electrolyzer stacks, along with their power, were determined using the mixed-integer linear programming (MILP) method. The system curtails the PV power when it exceeds the maximum power of the electrolyzers. On a second approach, a battery-assisted system was tested using different battery technology. The main conclusion is that the cheaper option is to allow curtailment, at the expense of not producing hydrogen continuously [15].

As with directly-coupled systems, the genetic algorithm appears in literature as an optimization tool, for example, in Ref. [10]. The authors used the genetic algorithm to vary the number of PV and electrolyzer cells in series and parallel and obtain optimum solutions defined by four objective functions related to cost and efficiency. For the DC-DC coupled system the topology of the converter was also analyzed finding that the optimum solution is sensitive to the converter topology.

A different approach for sizing the off-grid PV system powering an alkaline electrolyzer was followed in Ref. [16] by using the HOMER software to design the PV system and battery bank. They considered the load profile of a glass-producing factory and the solar resource in Algeria, where the project is located. The study resulted in 1 MW_p of fixed-axis PV with more than 100 batteries. The PV system is fully powering the whole plant, not only the electrolyzer but also the auxiliary systems.

A grid-connected PV system powering a fictitious alkaline electrolyzer plant in Türkiye was studied in Ref. [17]. The optimization method was the Generic Optimization algorithm (GenOpt) coupled with the simulation software TRNSYS. The objective was to minimize the electricity withdrawn from the grid by tuning the azimuth and tilt of the PV modules [17]. Setting either the electrolysis technology or the electrolyzer capacity as decision variables also allows minimizing energy taken from the grid and meeting production goals at minimum cost [18].

Piveta et al. [19] used MILP to minimize the cost and CO_2 emissions of a grid-connected PV system that provides electricity to a simulated hydrogen production facility in north-eastern Italy. They achieved the optimization objectives by tuning the PV, electrolyzer and storage tanks and using the grid and production targets as constraints. The minimum found Levelized Cost of Hydrogen (LCOH) was 7.8 €/kg_{H_2} for a system supplying hydrogen to a steel plant and a hydrogen refueling station with a 341 kW_p of PV and 89 kW PEM electrolyzer. Similarly, Engstam et al. determined the operating conditions for a grid-connected hydrogen facility in Sweden which minimize the LCOH and CO_2 [20]. The grid model is a multi-country system, and while this model does not aim to sizing, it demonstrates that the LCOH, and carbon emissions are greatly influenced by the operative decisions [20]. For directly coupled systems, the LCOH is a function of the ratio between PV and electrolyzer capacities with a single minimum [21,22].

Table 1 summarizes the selected optimization methods reported in the literature. Note that this list can be considerably expanded for directly coupled systems, as in the literature review of [23].

1.2. *Relevance of this study*

While the literature studies (Table 1) have focused on sizing studies, there is a clear gap in the design of stand-alone, DC-DC coupled (indirect coupled) systems. Furthermore, the strategies of direct coupling systems imply that the design of either, or both, components, PV and electrolyzers must be tailor-made for a particular system, because their number of cells and connection are used as decision variables. This prevents the use of readily available components. Grid-connected systems have different optimization objectives

Table 1 – Comprison of optimization methods found in literature. Indirect methods refer to DC-DC coupled systems. *MILP* stands for *Mixed Integer Linear Programming*, *PV for photovoltaic*, *EL for electrolyzer* and, *GenOpt for Generic Optimization*.

Ref.	Coupling	Optimization tool	Optimization objective	Decision variables
[3]	Direct	Statistical	MPP coupling	series EL & PV cells
[7,14,21,24,25]		Analytical	Efficiency, MPP coupling, cost	series-parallel EL & PV cells
[9,11–13,26]		Metaheuristic	Cost, H_2 production, efficiency, losses	Series-parallel EL & PV cells; EL temperature; water activity
[10]	Direct & indirect	Metaheuristic	Cost, H_2 production, losses; efficiency	Series-parallel EL & PV cells
[27]		Analytical	Cost, efficiency, H_2 production	PV & EL size & capacity
[15]	Indirect	MILP	System cost	EL power & battery type
[17]	Grid	GenOpt	Grid electricity	PV azimuth &tilt
[18–20]		MILP	Cost & CO_2 emissions	PV peak power, EL power, EL technology, Power flows in European countries

and constraints which are also not suitable for stand-alone systems.

The study of Gillisen et al. [15] is one of the few focusing on readily available components at an industrial scale focusing on indirectly coupled, stand-alone systems.

The purpose of this study is to develop an optimization procedure for a stand-alone PV-alkaline electrolysis system. The output of such procedure is a relative sizing factor, which gives a better insight on the relation between the size of the PV plant and the size of the electrolyzer, as well as the azimuth and tilt of the PV modules, which are often overlooked.

These are typically optimized for the PV production, or decoupled in the optimization process. While the tilt of PV modules is explored in Ref. [17] as a decision variable for grid-connected systems and in Ref. [27] as an analysis of its effect, these variables have not been used to size off-grid solar-hydrogen systems. In addition, this work considers that the load is not only the electrolyzer but also a compressor, which needs to be also powered by the PV system in a stand-alone system. Using a metaheuristic approach allowing the optimization of complex and diverse objective functions.

The model used, although programmed in MATLAB, can be easily translated into any programming language that supports the Particle Swarm Optimization algorithm (e.g. Refs. [28,29]).

Determining of the orientation of the PV modules, the focus on a fully autonomous system and the inclusion of a compressor to model the balance-of-plant form the main contributions of the present work.

The rest of this paper is structured as follows. Section 2 proposes the system description and models of the electrolyzer and compressor. This is extended in Section 3 with the optimization procedure. The results and analysis are discussed in Section 4 before closing with the conclusion in Section 6.

2. System model

The studied model consists of an off-grid PV system coupled to an alkaline electrolyzer using a DC-DC converter. A compressor is added as a Balance-of-Plant component. Fig. 1 illustrates the studied system.

2.1. *Electrolyzer model*

The electrolyzer in this work was assumed to be of alkaline technology with a nominal power of 100 kW, and modeled with Ulleberg's model [30]. This model assumes that the total cell voltage is a sum of the reversible voltage and the overvoltage caused by resistive effects and activation of the electrodes.

$$V_{cell} = V_{rev} + V_{ohm} + V_{act} \quad (1)$$

The reversible voltage V_{rev} is the minimum voltage needed to start the decomposition of water. It is related to the change of Gibbs free energy, ΔG, and is a function of temperature. At 25 °C and 1 atm (standard conditions), $\Delta G^0 = 237.2$ kJ/mol, which is equivalent to $V_{rev} = 1.229$ V [31]. The ohmic losses V_{ohm} represent the losses at the electrolyte, electrodes, and

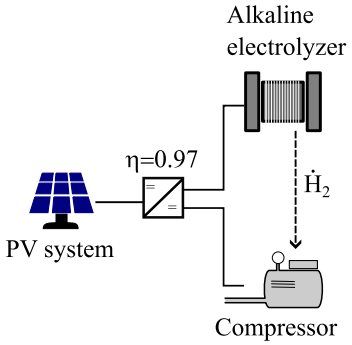

Fig. 1 – Description of the studied system. The solid line represents the electrical connection between components, while the dashed line indicates the flow of hydrogen.

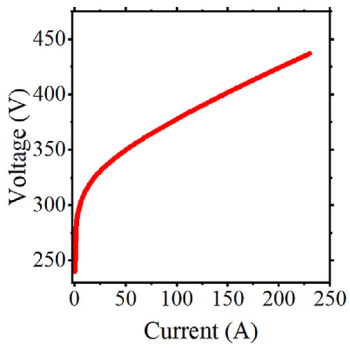

Fig. 2 – Current-Voltage curve of the simulated alkaline electrolyzer.

bubbles, while the activation losses, V_{act}, model the overpotential caused by the energy needed to start the reaction. This is often described with the Butler-Volmer equation, or one of its simplifications [32]. The activation overpotential has a logarithmic dependency on the applied current.

Equation (2) shows the semi-empirical equation to describe the electrolyzer voltage as a function of the applied current density i (in A/m^2) and the operating temperature (in °C) [30].

$$V_{cell} = V_{rev} + ri + s\log(ti + 1) \tag{2}$$

The current density normalizes the applied current to the electrolyzer, I, by the cell area (A): $i = I/A$. The terms r and t are coefficients linked to the resistivity of the separator and the exchange current density respectively. The latter is related to the charge transfer between the electrodes in an open circuit condition [33]. Both r and t are temperature (T) dependent, as seen in Equations (3) and (4). The coefficient s is linked to the Tafel slope. Note that the r_x, t_x, and s terms are fitting parameters [30].

$$r = r_1 + r_2 T \tag{3}$$

$$t = t_1 + t_2/T + t_3/T^2 \tag{4}$$

The values for the parameters were taken from Ref. [34] and shown in Table A.1 of the appendix.

Equation (2) defines the voltage of a single electrolyzer cell; however, for a stack of cells, it is assumed that all the cells are identical and connected in series. The total voltage of the stack V_{ele} is the number of cells (N_{cells}) multiplied by the voltage of a single cell (V_{cell}). Fig. 2 shows the simulated I–V curve. Constant temperature of 60 °C and 186 series-connected cells were assumed. The reason for this is to simulate an industrial-sized electrolyzer. The I–V model used here is reproduced from Ref. [34] where the I–V curve of a small-scale electrolyzer was demonstrated to be scalable to an industrial size with an electrolyzer of 186 cells. This number allows the results to be traceable and comparable.

According to Faraday's law of electrolysis, the hydrogen flow, $\dot{H}_2$, is proportional to the current applied to the electrolyzer, I as in Equation (5).

$$\dot{H}_2 = \eta_F \frac{I}{2F} \tag{5}$$

The term η_F accounts for the difference between the theoretical rate of production and the real one, and is called the Faraday efficiency. For simplification, $\eta_F = 1$. F is Faraday's constant, indicating the electric charge of 1 mol of electrons (F = 96,485 C/mol).

The alkaline technology cannot operate below 20% of its nominal current to avoid gas crossover from the oxygen to the hydrogen chamber. This, if happens, can result in an unsafe situation [30]. For this reason, whenever the PV power, P_{PV}, is insufficient to meet the minimum power demand of the electrolyzer, P_{min}, the system will be switched off. When the PV power exceeds the nominal power of the electrolyzer, P_{nom} it will be curtailed to the nominal power of the electrolyzer. The conditions are expressed in Equation (6).

$$\begin{cases} P_{ele} = 0, & P_{PV} < P_{min} \\ P_{ele} = P_{nom}, & P_{PV} > P_{nom} \\ P_{ele} = P_{PV}, & \text{otherwise} \end{cases} \tag{6}$$

2.2. Compressor model

The compressor is modeled as an isentropic process. The main assumption is that the hydrogen behaves as an ideal gas and there is no heat transfer from the gas to the structure of the compressor or the ambient. From these assumptions and applying the First Law of Thermodynamics, the work (W) needed to compress hydrogen at constant volume is the change of enthalpy (H) of the gas as seen in Equation (7). The change of enthalpy can be obtained from the specific heat of hydrogen at constant pressure (C_p), the difference of temperature at the inlet (T_1) and outlet (T_2) of the compressor, and the amount of gas involved (n) [35,36].

$$W = n\Delta H = nC_p(T_2 - T_1) \tag{7}$$

The law of ideal gases is recalled in Equation (8). This equation describes the behavior of the amount of gas (n) at given pressure (P), volume (V), or temperature (T). R is the universal gas constant with a value of 8.314 J mol^{-1}K^{-1}.

$$PV = nRT \tag{8}$$

For an isentropic compression process, the entropy remains constant, and the relation between the input and

output pressures is given by the Compression Pressure Ratio (CPR) as in Equation (9) [37].

$$\mathrm{CPR} = \frac{P_2}{P_1} = \left(\frac{T_2}{T_1}\right)^{\gamma/(\gamma-1)} \tag{9}$$

The term γ is the ratio of the specific heats at constant pressure C_p and constant volume C_v (Equation (10)). The latter can be derived from the former using the fact that the universal gas constant, R, is the difference of both specific heats ($R = C_p - C_v$) [37].

$$\gamma = \frac{C_p}{C_v} \tag{10}$$

Under ideal conditions, the electrical power to compress hydrogen (w_c) is the same as the work applied to the gas (Equation (7)) per unit of time. To consider non-idealities, an efficiency term needs to be considered ($\eta = 0.6$ [14]). Working out Equation (7) 8, 9, and 10 leads to the expression for the electric power needed by the compressor (Equation (11)) [14].

$$w_c = C_p \dot{H}_2 \frac{T_1}{\eta}\left(\mathrm{CPR}^{(\gamma-1)/\gamma} - 1\right) \tag{11}$$

Note the term $\dot{H}_2$ which is the hydrogen flow in kg/s defined in Equation (5). It results from replacing n with $\dot{H}_2$ in Equation (8). This allows the calculation of electric *power* instead of *energy*. This model is typically applied in describing PV-hydrogen systems as in Ref. [14]. Table A.2 in the appendix shows the used values for the model.

2.3. PV model

The production of the PV system was calculated using data from the Royal Meteorological Institute of The Netherlands [38]. This data was collected in 2013 in Cabauw, a small town located in the center of The Netherlands. The dataset contains 1-min resolution irradiance values including Global Horizontal Irradiance (GHI), Diffuse Horizontal Irradiance (DHI), Direct Normal Irradiance (DNI) and, ambient temperature.

The PV system is assumed to be installed on flat ground, with free horizon. Further, all the PV modules receive the same irradiance, and there is no partial shading either from clouds, self-shading or any other obstacle.

The total irradiance that the PV module receives (G_m) is needed to calculate the instantaneous PV power. G_m is the sum of direct (G_{dir}), diffuse (G_{diff}) and reflected (G_{ref}) irradiance components as seen in Equation 12

$$G_m = G_{dir} + G_{diff} + G_{ref} \tag{12}$$

The direct irradiance on a tilted surface (PV module) can be obtained from the DNI by calculating the angle of incidence (AOI) between the Sun (described by its altitude in degrees above the horizon, a_s, and its azimuth in degrees starting from the North, A_s) and the normal vector of the PV module (described by the module's tilt, a_m and azimuth A_m) as shown in Equations (13) and (14) [39].

$$\cos \mathrm{AOI} = \cos a_m \cos a_s \cos(A_m - A_s) + \sin a_m \sin a_s \tag{13}$$

$$G_{dir} = \mathrm{DNI} \times \cos \mathrm{AOI} \tag{14}$$

The diffuse irradiance seen by this (tilted) PV module (G_{diff}) was obtained from the DHI considering an isotropic sky model (Equation (15)) [39].

$$G_{diff} = DHI \times \frac{1 + \sin a_m}{2} \tag{15}$$

A tilted module also receives reflected irradiance from the ground which is affected by the albedo (α) of the site. A constant value of the albedo of 0.2 was assumed (Equation (16)).

$$G_{ref} = DHI \times \alpha \times \frac{1 - \sin a_m}{2} \tag{16}$$

The Normal Operating Cell Temperature (NOCT) model accounts for the temperature effect, which models the difference between the temperature of the solar cell (T_m) and the ambient temperature (T_a) as a linear function of the incident irradiance on the PV module (Equation (17)) [39].

$$T_m - T_a = \frac{T_{NOCT} - 20}{800} G_m \tag{17}$$

The term T_{NOCT} in Equation (17) refers to the solar cell temperature when the module is exposed to an incident irradiance of 800 W/m^2 and 20 °C ambient temperature with 1 m/s wind speed [40]. This value is given in the datasheet of manufacturers.

Fig. 1 shows that the PV module is connected to a DC-DC converter. This converter performs maximum power point tracking (MPPT), which implies that, at every instant, the instantaneous PV power is the PV module's maximum power under the instantaneous irradiance. This assumption simplifies the calculation as it does not require knowledge of the module's IV curve. The module's MPP (instantaneous PV power) is then equal to the received irradiance multiplied by the efficiency of the module (given in the module's datasheet) corrected for temperature and irradiance effects and the module's area (Equation (18)) [39]. At standard test conditions, the maximum power point, P_{mpp}, the open circuit voltage V_{oc}, and the module's efficiency, η, can be obtained from the module manufacturer's datasheet as well as the module's area A_{module} and the deviation of the maximum power point as the temperature changes, α_p. The parameter $n_d = 1.5$ is the ideality factor of the diode. The technical specifications of a Trina Tallmax M 450 W$_p$ module [41] were considered.

$$\eta_{Tm,Gm} = \frac{P_{mpp}}{1000 A_{module}}\left(1 + \frac{0.0258 n_d}{V_{oc}} \times \ln\left(\frac{G_m}{1000}\right)\right)\left(1 + \frac{1}{\eta}\frac{\partial \eta}{\partial T}(T_m - 25)\right)$$
$$\frac{\partial \eta}{\partial T} = \frac{P_{mpp} + \alpha_p (T_m - 25)}{(1000 A_{module})(T_m - 25)} \tag{18}$$

The PV power was further reduced by 97% to account for the losses at the DC-DC converter (semi-ideal behavior, considering a constant efficiency of 0.97 over the whole power range. This number was chosen after an analysis with the model proposed in Ref. [42]).

3. Optimization procedure

The optimization consists on finding the values of the decision variables that minimize the objective function. In this case, the decision variables are the azimuth of the PV modules, their tilt, and the oversize factor (i.e., ratio between the PV system peak power to the nominal power of the electrolyzer). The objective functions are the cost, specific energy use and specific wasted energy, explained in Section 3.3. The Particle Swarm Optimization (PSO), (discussed in Section 3.1) is the tool used for finding the optimal values. For each iteration of PSO, the following steps are taken:

1. Calculate the theoretical instantaneous power of the PV system without load.
2. Distribute the PV power to the electrolyzer and compressor (discussed in Section 3.2.
3. Integrate the instantaneous values over the whole year and calculate the performance indicator (Section 3.3) to be optimized (objective function).

The next section explains the aforementioned steps in detail.

3.1. *Particle swarm algorithm (PSO)*

The Particle Swarm Optimization (PSO) is an algorithm based on the interactions between individuals in flocks of birds or school of fish [43]. It relies on the concept of *particles*, which are associated to solutions of the objective functions [44]. Each individual, or *particle*, is described by its position in the search space (i.e. the possible values for the decision variables) and a velocity, an updatable parameter that controls how fast this particle moves toward the rest of the individuals. Additionally, the particles have a memory of themselves and the rest of the group. This means that a particle keeps a record of the best solution it has found over all the iterations, and also knows the best solution of all the individuals in the swarm [43]. The algorithm starts by creating a population of individuals randomly distributed over the search space, with initial position and velocity. The objective function is calculated for every particle and the individual best and group best parameters for each particle are updated. If a particle finds a solution that is lower than the record of its individual best, it replaces its parameter with the new found solution. The same applies to the group best parameter. The position and velocity parameters of each particle are updated and then, all the particles are again randomly replaced. But, this new placement depends on the previous position, velocity, and individual and group bests. In this way, all the particles begin to move towards the global minimum of the objective function [43,44].

PSO performs better than other metaheuristic algorithms (genetic algorithm and imperialist competitive algorithm) when optimizing directly-coupled systems. It is faster, finds the optimum in fewer iterations and converge to the global minimum [45].

3.2. *Power distribution*

As a completely stand-alone system, the PV system (P_{PV}) must provide all the electricity needed to operate the electrolyzer P_{ele} and the compressor P_{comp} as seen in Equation (19).

$$P_{PV} = P_{ele} + P_{comp} \tag{19}$$

This implies that not all the power of the PV system is available to produce hydrogen. Hydrogen production is proportional to the applied current to the electrolyzer I_{stack} as discussed in Section 2.1. The Newton-Raphson method shown in Equation (20) was used to calculate this amount.

$$I_{stack_{n+1}} = I_{stack_n} - \frac{f(I_{stack_n})}{f'(I_{stack_n})} \tag{20}$$

The subindices $n+1$ and n are the updated and current values of the current, respectively. As this is an iterative process, the updated value will be used as the current value in the next iteration. Equation (21) shows $f(I_{stack})$ which is the function of the electrolyzer current whose root is precisely the current which ensures that the power balance (Equation (19)) is valid. This equation was obtained from the power of the electrolyzer, calculated as the product of its voltage and current $P_{ele} = V_{ele} \times I_{stack}$. Note that the electrolyzer's voltage (Equation (2)) is a function of the electrolyzer's current, I_{stack}, hence, P_{ele} is also a function of this variable. The hydrogen flow, which is also dependent on I_{stack} (Equation (5)), is the link between the electrolyzer and the compressor because the compressor power (Equation (11)) is governed by the hydrogen flow, and subsequently, by the electrolyzer current. The power balance can be written in terms of I_{stack} because both the electrolyzer and compressor powers can be expressed in terms of the electrolyzer current. Equating the resulting expression to zero leads to Equation (21) which is the expression of $f(I_{stack})$. The coefficient 2.016×10^{-3} kg/mol is the molar weight of hydrogen and is included to ensure the match of the units. The term K_1 is defined in Equation (22) and it is used to simplify the expressions in Equations (21) and (23). With the assumptions described in Section 2, K_1 is a constant.

$$f(I_{stack}) = \frac{s}{\ln 10}\ln\left(\frac{t}{A}I_{stack}+1\right)I_{stack} + \frac{r}{A}I_{stack}^2 + \left(\frac{2.016\times10^{-3}\times K_1}{2F} + V_{rev}\right)I_{stack} - \frac{P_{PV}}{N_{cells}} \tag{21}$$

$$K_1 = \frac{C_p T_1}{\eta}\left(CPR^{(\gamma-1)/\gamma} - 1\right) \tag{22}$$

$f'(I_{stack})$ (Equation (23)) is the derivative of this function with respect to I_{stack}, which is needed in the Newton-Raphson method.

$$f'(I_{stack}) = \frac{s}{\ln 10}\left[\frac{t}{tI_{stack}+A}I_{stack} + \ln\left(\frac{t}{A}I_{stack}+1\right)\right] + \frac{2r}{A}I_{stack} + \frac{2.016\times10^{-3}\times K_1}{2F} + V_{rev} \tag{23}$$

3.3. Performance indicators

Three performance indicators evaluate the system. These indicators were used also as objective functions.

The *specific energy use* of the system was defined as Equation (24). This indicator is a measure of the efficiency of the system, because it relates the energy that could be produced from the PV system ($\int_{year} P_{PV}$) to the amount of hydrogen that was actually produced $\int_{year} \dot{H}_2$. The units are in kWh/kg_{H_2}.

$$\text{Energy use} = \frac{\int_{year} P_{PV}}{\int_{year} \dot{H}_2} \tag{24}$$

A closely related indicator is the *specific wasted energy* and contains two components: the *unused energy* and the *curtailed energy*. These indicators arise from the operational limits of the electrolyzer defined in Section 2.1. The unused power, P_{unused}, is the power that could be generated from the PV system, but it is not, as a result of the electrolyzer being off due to insufficient power to meet the operating limits. The curtailed power, $P_{curtailed}$, is defined analogously, as the energy that could be generated from the PV but it is bounded to meet the maximum operating limit of the electrolyzer. The wasted energy is then defined as Equation (25).

$$\text{Wasted energy} = \frac{\int_{year} (P_{unused} + P_{curtailed})}{\int_{year} \dot{H}_2} \tag{25}$$

The Levelized Cost of Hydrogen (LCOH) is the third and last indicator. It represents the cost of producing 1 kg of hydrogen (€/kg_{H_2}). Equation (26) [46] was used to calculate the LCOH. The numerator is the sum over every year, t, of all the installation costs of the system I_t incurred during the lifetime of the project ($n = 25$ years) plus the maintenance and replacement costs, M_t. The denominator is the yearly production of hydrogen H_t. The term $\frac{1}{(1+r)^t}$ is the annuity factor to consider for the future value of the costs and is calculated with the interest rate, $r = 4\%$ (which is in line with the sensitivity analysis carried out by Ref. [47]), and the year of the calculation, t. The values used for the calculation of the LCOH are given in the appendix, Table A.3.

$$LCOH = \frac{\sum_{t=0}^{n} \frac{I_t + M_t}{(1+r)^t}}{\sum \frac{H_t}{(1+r)^t}} \tag{26}$$

4. Results and discussion

4.1. Optimization results

Two types of PV systems were studied. First, one with all modules oriented at the same azimuth and tilt, and second, a PV system whose half of the modules are flipped 180° in azimuth with respect to the first half, but the tilt is the same for both halves. This second system opens the possibility for the optimization of east-west oriented modules.

Ten runs were carried out for each indicator for each PV system to check for convergence of the optimization procedure. Fig. 3a,b shows the optimization results for the orientation of the PV modules of single and double orientations, respectively. Fig. 3c shows the resultant oversize factor for each type of the PV systems as a function of the objective functions.

From Fig. 3a it is possible to note that the PSO found that the configurations which minimize the specific energy use are facing north. As a reminder, the PV system is assumed to be installed in The Netherlands, in the northern hemisphere, and the expected best azimuth is facing southwards. Even more remarkable is the fact that the north-facing modules are not horizontal (as would be expected to compensate for the north-facing azimuth). This means that the PV modules are oriented away from the Sun. When looking at Fig. 3c, this configuration corresponds to the upper limit set for the oversize factor. This is needed to compensate for the fact that the north-facing PV system harvests only diffuse irradiance. The minimization of the wasted energy with a single orientation also results in north-facing PV modules. Although the oversize factor does not reach its limits. One of the configurations that minimize the wasted energy results in almost horizontal modules, which are associated with a lower oversize factor (Fig. 3c).

Another interesting observation is that, for single-sided systems, the angle that maximizes the PV production is not the same as the one that optimizes any of the indicators. This is relevant because typically, the PV system is optimized first for maximum energy production; then, the electrolyzer is selected.

Fig. 3b shows the case of the double-sided configuration. For the energy use, PSO found configurations in the North-South orientation. As opposed to the single-sided version, where all the modules receive only diffuse irradiance, in the double-sided version, half of the PV modules are actually facing south.

To minimize the hydrogen cost with a two-sided system, the modules should be placed horizontally. Under this situation, the azimuth does not play a role anymore (as seen in the wide range of azimuth values for LCOH in Fig. 3b). This is the only case where the orientation for a particular indicator (LCOH in this case) matches the optimal angle for PV generation. The oversize factor remains almost the same for both configurations (2.58 and 2.82 for single and double-sided, respectively) (Fig. 3b).

The double-sided analysis was performed to study the possibility of installing the PV modules in an East-West configuration. However, PSO did not find this orientation favorable for any indicator.

The calculation of the indicators of each configuration offers a better insight into the effect of the configurations. The selection of these configurations is based on the results of Fig. 3 and are, two for minimizing energy use, two for the LCOH (one for each type of PV system), and three for wasted energy (2 single-sided and one double-sided). The used values are given in Table 2.

Fig. 4 shows the value of every indicator for each configuration of Table 2. The minimum hydrogen cost is obtained with configuration *LCOH 1*, which is a south-facing, single-sided arrangement. The two-sided configuration did not offer

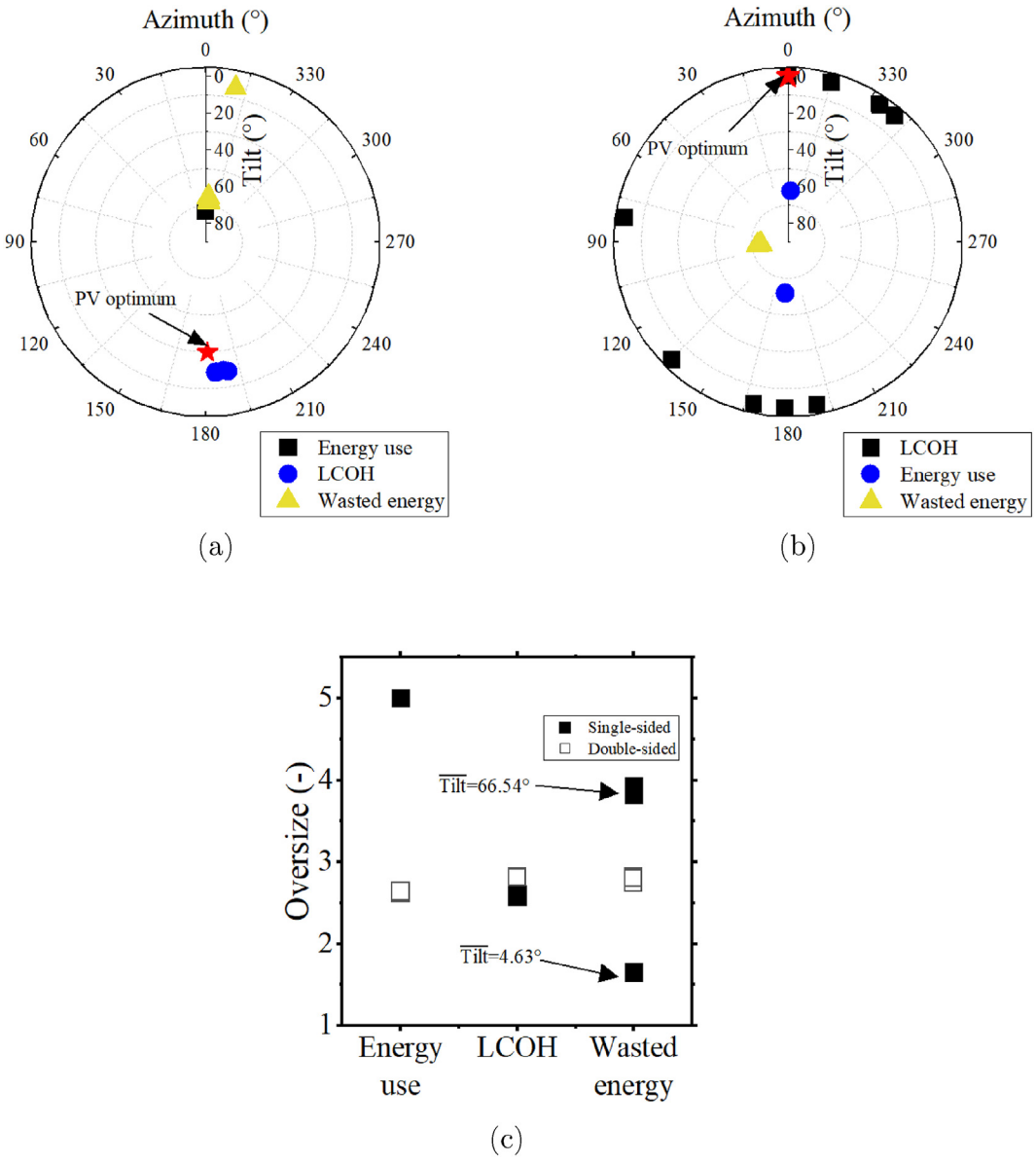

Fig. 3 – Optimization results for orientation and oversize factor. Ten runs were carried out. Each point represents one of the runs. Note that in many cases the points are overlapping, indicating convergence of PSO. (a) Single-sided configuration (All PV modules have the same azimuth and tilt). The orientation that maximizes the yearly PV energy is marked with a star. (b) Double-sided configuration (Half of the PV modules are displaced 180° in azimuth with respect to the first half. All modules share the same tilt). (c) Oversize factor for all indicators and both PV configurations. The arrows that are labeled with $\overline{\text{Tilt}}$ mark the average tilt of the pointed clusters.

Table 2 – Selected configurations. O.F. stands for "oversize factor" and "#PV" for the number of PV modules.

Indicator	PV system	Azimuth (°)	Tilt (°)	O·F.	# PV	Abbreviation
Energy use	single	0.3	73.4	5	1111	Efficiency 1
	double	176.83	62.16	2.63	584	Efficiency 2
LCOH	single	184.5	18.9	2.58	573	LCOH 1
	double	243.07	0.0	2.82	627	LCOH 2
Wasted energy	single	355.98	66.54	3.86	858	Wasted 1
		348.94	4.63	1.65	367	Wasted 1H
	double	95.2	74.66	2.80	622	Wasted 2

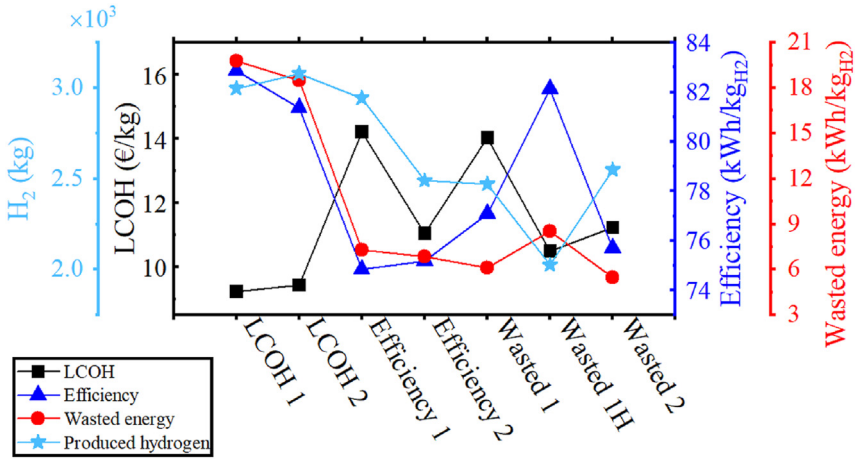

Fig. 4 – Evaluation of the different configurations with every indicator. The abbreviations on the horizontal axis correspond to those mentioned in Table 2

any advantage for the hydrogen cost. But a horizontal placement of the PV modules opens the possibility of reducing energy consumption, and wasted energy while boosting hydrogen production with just a small increase in the price. It can be even more attractive because the increase in PV size is not significant.

It is no surprise that the higher costs correspond to the north-facing configurations.

Note that the energy consumption calculated here also considers the curtailed energy. And for this reason, the obtained values are higher than the expected values for energy consumption for alkaline technology, which are in the range of 50 kWh/kg_{H_2} [48].

Authors in Ref. [49] found an optimal oversize ratio of 1.4 on average to minimize the hydrogen cost. They compared the performance of 18,500 commercial PV modules and perform the optimization with the number of PV modules as a decision variable. In the same direction, the oversize ratio which minimizes the LCOH of a stand-alone PV-hydrogen system located in Townsville, Australia was 1.5 [22], while the oversize factor obtained from this study is around 2.5. One potential reason for this difference can be attributed to the energy needed by the compressor. Another important difference is the geographical location (Algeria [49] and Australia [22]) with a higher irradiance than The Netherlands. The optimal oversize factor changes depending on the capacity factor of the PV plant, linked to the solar resource available per location [21]. Lastly, the fact that the orientation is also taken into account influences the oversize factor compensating for lower generation from the PV system.

The efficiency is sensitive to the tilt of the PV modules, as demonstrated by the results and also reported in Ref. [27]. As opposed to Ref. [27], whose optimal tilt is 60°, the highest efficiency occurs when the PV modules are vertical. The difference in efficiency values can be attributed to a) location (Rome [27], and The Netherlands (this study)), b) the consideration of the oversize factor and azimuth of the PV modules and c) The sensitivity of PSO to the imposed limits to the oversize factor (see Appendix A.2).

Albeit the three defined indicators, reliability (expressed with the loss of load probability), economic (net present cost, LCOH, capital recovery factor), and environmental (CO_2 emisions and energy emission factor) are other indicators discussed in the literature for stand-alone hydrogen-based systems [50].

4.2. *Operation at partial load*

A load duration curve is a tool frequently used in electrical engineering to represent the time (horizontal axis) that a load is expected (vertical axis) [51]. This tool facilitates the description of the operation at partial load of the alkaline electrolyzer. Fig. 5 shows the partial load duration curve of the electrolyzer when different configurations are used. These figures were obtained by calculating the instantaneous power delivered to the electrolyzer (following the procedure described in Section 3.2). This power, with a resolution of minutes, was resampled into hourly values by calculating the average of all powers within an hour. The hourly power values were normalized against the nominal power of the electrolyzer, sorted in descending order, and then plotted. Note that the graphs show an average of every hour. For this reason, the graph shows values below the minimum operating threshold.

Fig. 5a corresponds to the partial load operation of the electrolyzer when optimized for maximum efficiency (minimum energy use). The inset at the top right shows the portion of the graph when the electrolyzer operates at full load. In all cases, the electrolyzer operated for less than 100 h at full load. The single-sided, north-facing PV system has a better partial load characteristic than the south-facing PV system operating for an additional 390 h (inset, lower right corner).

For the configurations optimizing the LCOH, there is little difference in the partial load operation for single-sided and horizontally-placed PV modules. The latter allows the operation for 3 days more than with the former configuration, as seen in Fig. 5b. Observe that the electrolyzer operates at full-load for more time for the layout that minimizes the LCOH. This results in improved hydrogen production (Fig. 4).

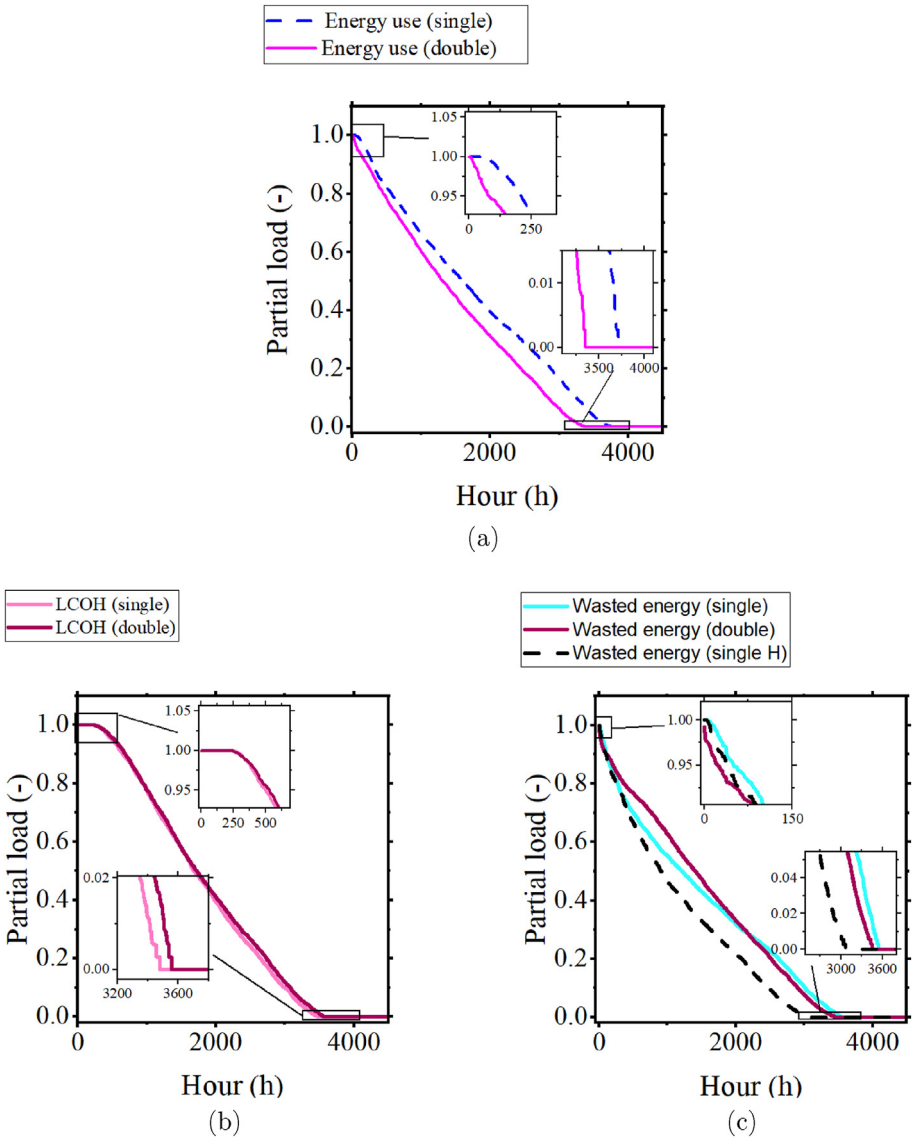

Fig. 5 – Partial load curves for the configurations of Table 2. (a) Efficiency (energy use). (b) LCOH. (c) Wasted energy.

The layout that minimizes the specific energy use (Fig. 5a) prioritizes the operation at lower loads rather than the full-load range. In fact, the electrolyzer only operates for a few hours at full capacity. A similar situation occurs with the configuration optimizing the specific wasted energy (Fig. 5c). The single-sided configuration with an almost horizontal module (*Wasted 1H*) leads to very poor use of the electrolyzer despite being the configuration with the lowest cost among those aiming at reducing the energy spill (wasted energy and energy use) as seen from Fig. 4.

The utilization of the PV system can be studied by looking at the histograms of the potential production for each configuration. The word *potential* is important because not all of the PV power can be used. As presented in Section 3.3, the electrolyzer imposes operative limits, and, whenever the PV power violates these boundaries, it must be curtailed. Fig. 6 illustrates the distributions of the PV power (P_{PV}). As a reference, the distribution of the GHI at the site is also included (Fig. 6a). A light blue rectangle marks the regions where the PV power is used by the hydrogen equipment (i.e., electrolyzer and compressor). From Fig. 6b and d it is possible to conclude that the PSO algorithm tries to minimize the curtailed energy (values above 112 kW of PV power). In doing so, it allocates more power to the low-production region. The power in this region cannot be used, and despite it being very small, the large occurrence results in more unused than curtailed energy.

The minimum LCOH is achieved with a more aggressive strategy. Fig. 6c illustrates that, in contrast to the other indicators, the PV layout for minimum LCOH attempts to harvest as much PV power as possible in the operating region of the hydrogen equipment. The trade-off is a considerable amount of curtailed energy.

A different electrolyzer technology, such as Proton-Exchange Membrane (PEM), with a higher dynamic range

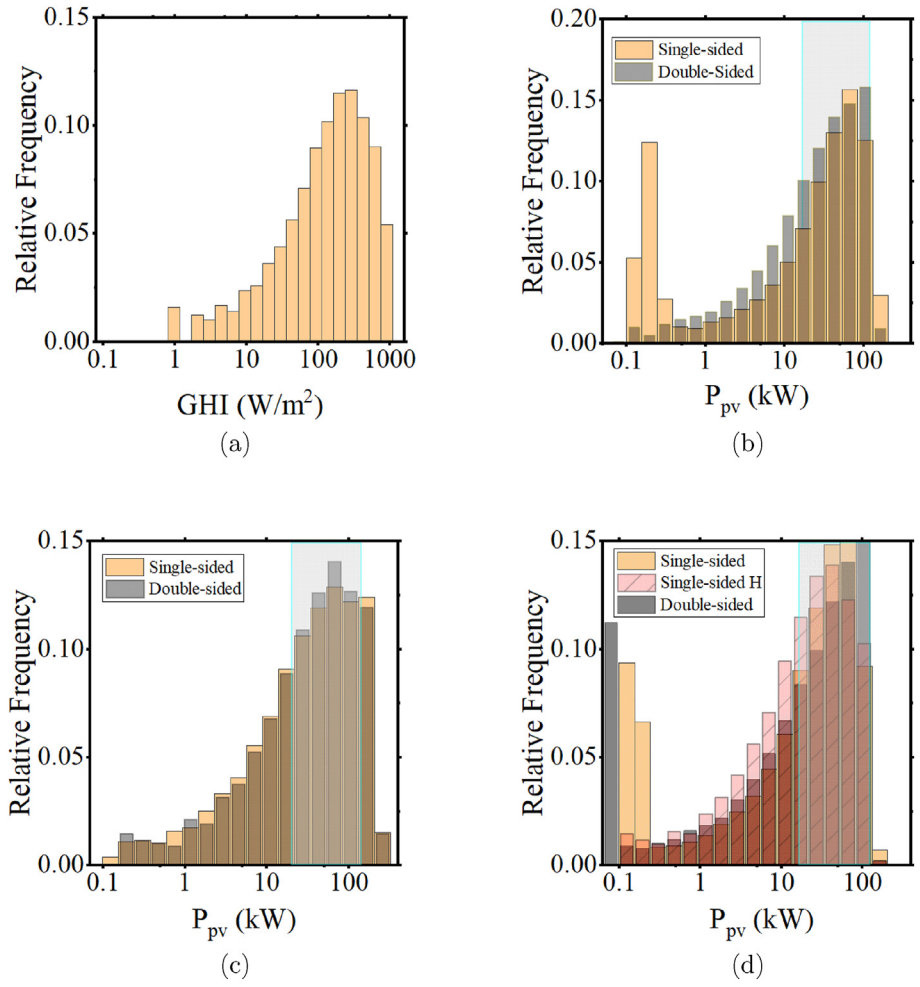

Fig. 6 – Histograms of the potential PV production for configuration optimizing each indicator. (a) Distribution of the GHI at the analyzed site. (b) PV power when the system is optimized for maximum efficiency (minimum energy use). (c) PV power when the system is optimized for minimum LCOH. (d) PV power when the system is optimized for minimum wasted energy. In graphs (b), (c), and (d), the light blue rectangle marks the operating region of the hydrogen equipment (electrolyzer and compressor). Observe that the horizontal axis in all figures is a logarithmic scale. (For interpretation of the references to colour in this figure legend, the reader is referred to the Web version of this article.)

(from 0 to 100%) [52], could improve the utilization of the PV power. The optimization for reducing the wasted energy already leads to very little curtailed energy (0.59 kWh/kg_{H_2} with a two-sided configuration). Most of the wasted energy in this configuration comes from the unused energy (Fig. 6d) which could be well absorbed by a PEM electrolyzer or multiple smaller units as in Ref. [2] or [53].

5. Sensitivity and uncertainty analysis

5.1. *Uncertainty analysis*

An uncertainty analysis on the convergence of PSO for each indicator ensures the validity of the presented results. The uncertainty analysis relies on the results from the ten runs carried out for each indicator, as discussed in Section 4 and shown in Fig. 3. The bootstrap resampling method offers an alternative to recalculating hundreds of new samples and was chosen because the optimization procedure is computationally expensive. The bootstrap uses the original ten optimization runs as the initial sample and allows to easily increase the sample size from 10 to 1000. Recall that the bootstrap is a resampling with replacement method is used to compute population statistics based on a small sample [54]. The median of each sample describes best the data. The mean is highly affected by outliers, assumed present in the samples. Then, the 95% confidence interval of the sample medians was calculated.

Table 3 shows the mean of medians of the 1000 bootstrapped samples. The 95% confidence interval limits are a measure of uncertainty. There is a 95% probability that the true median is found within the confidence interval limits. Note that there are four significant digits to show that, in

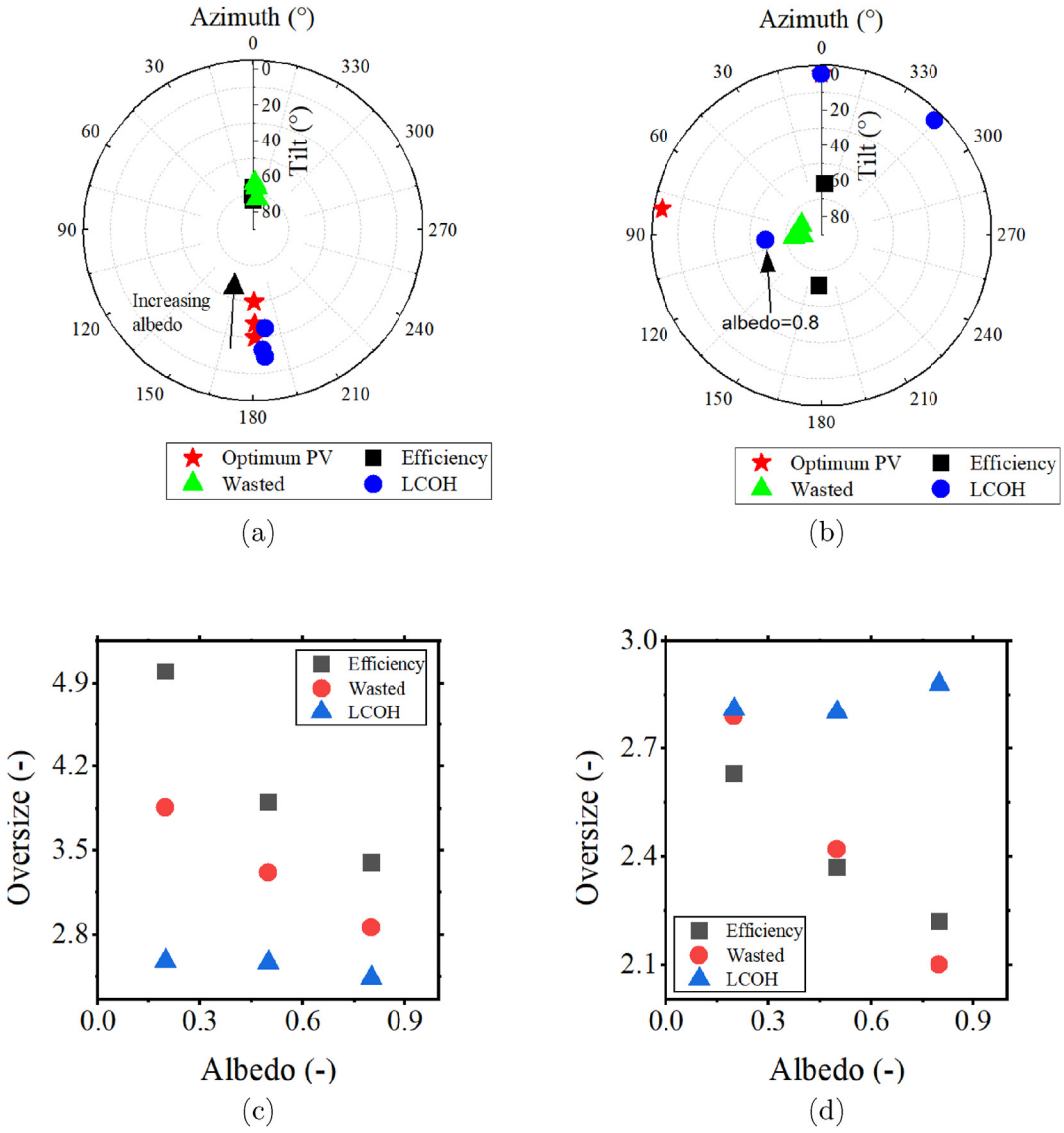

Fig. 7 – Sensitivity analysis of the albedo modeling parameter. The selected albedo values are 0.2, 0.5 and 0.8 (unitless). (a) PV module orientation of single-sided system. The arrow shows that the optimal tilt for PV production increases with albedo. (b) PV module orientation of a two-sided system. The arrow points a highly tilted east-west orientation. (c) Oversize factor of the single-sided system, and (d) oversize factor of the double-sided system.

general, the confidence intervals are tight, indicating that the variables tend to converge to the same value, leading to a stable median. The azimuth has the highest uncertainty, especially in the double-sided efficiency and LCOH. This high uncertainty comes from the fact that for the double-sided efficiency, PSO found two opposite configurations, one pointing north and one south. Although this might seem contradictory, when analyzing the deviations, it is possible to see that the offset is almost 180° (same as the difference between the low and high confidence interval limits for this configuration), and only for a double-sided system, as defined in this work, north-facing and south-facing are equivalent. The other situation with very high uncertainty is the azimuth for the double-sided LCOH. The high dispersion of values can be explained when looking at the *tilt* for this configuration. It can be stated with very high confidence, that the modules are horizontal, and, under this situation, the azimuth has no influence on the PV output. Omitting these two scenarios, the highest deviation for the azimuth is 1.92° and 2.15° for the tilt. With respect to this last variable, Fig. 3 shows one value that did not converge to the median. With the uncertainty analysis, it is safe to label this point as an outlier, as it is beyond 1.5 times the interquartile range and has a negligible effect on the position of the sample median. The maximum deviation of the oversize factor is 0.0743. This means that the PV installation will have an uncertainty of ±17 commercial PV modules (450 W).

Table 3 – Mean of medians of 1000 bootstrapped samples. "CI low" and "CI high" are the 95% confidence interval for the low and high limits, respectively.

Indicator	Variable	Median	CI low	CI high
Efficiency single side	Azimuth (°)	0.3701	0.2476	0.4357
	Tilt (°)	73.3787	73.3735	73.4190
	Oversize (–)	5.0000	4.9999	5.0000
Efficiency double side	Azimuth (°)	196.3287	176.7190	356.8274
	Tilt (°)	62.2008	62.1838	62.3933
	Oversize (–)	2.6357	2.6305	2.6390
LCOH single side	Azimuth (°)	184.7602	184.3911	186.3103
	Tilt (°)	18.8621	18.6695	19.0356
	Oversize (–)	2.5777	2.5740	2.5907
LCOH double side	Azimuth (°)	253.5580	157.1478	335.5511
	Tilt (°)	0.0005	0.0000	0.0031
	Oversize (–)	2.8178	2.8148	2.8215
Wasted single side	Azimuth (°)	355.9400	355.6708	356.2193
	Tilt (°)	65.9232	65.5979	67.7439
	Oversize (–)	3.8381	3.8261	3.9005
Wasted double side	Azimuth (°)	95.0952	94.9564	95.4597
	Tilt (°)	74.6581	74.3982	75.1216
	Oversize (–)	2.7984	2.7948	2.8050

5.2. *Sensitivity of the model parameters*

The modeling parameters influence the PV and hydrogen production calculation, leading to potential deviations of the results if these are chosen incorrectly. To determine the extent of these deviations, a sensitivity analysis was performed changing the site's albedo, the operating temperature, and the compression ratio. For the last two, the obtained configurations only change slightly, while for the albedo, has a more significant effect. Fig. 7 shows the orientation for single (Fig. 7a) and double (Fig. 7b) sided orientations when changing the assumed albedo from 0.2 to 0.5 and 0.8. The results for the oversize are shown in Fig. 7c (single-sided) and 7d (double-sided).

For single-sided systems, the albedo modifies the tilt of PV modules, which is expected, as they harvest more reflected irradiance. This has a consequence on the optimal configurations for LCOH which follows the same trend (more vertical installations), but is negligible for energy consumption and wasted energy. The opposite occurs with the oversize factor. The LCOH remains almost constant, while the oversize for efficiency (energy consumption) and wasted energy decreases dramatically. This can be attributed to the considerably high tilt of the PV modules. Under this situation, they receive more reflected irradiance, even when facing north.

For a double-sided system, the results remain almost the same. Note that, in Fig. 7b, the efficiency results remain the same, even when there are opposite azimuths. Remember that the modules are back-to-back, making all efficiency results of Fig. 7b equivalent. For the LCOH, two of the three configurations are horizontal making the azimuth of the PV modules irrelevant.

An interesting observation is that with a large albedo (0.8) the configuration for the LCOH changes dramatically, from horizontal to a vertical East-West one with a slight increase in the plant size (Fig. 7c).

The optimization procedure is also sensitive to the computation parameters, especially to the upper limit imposed on the oversize factor, as this forces PSO to find new configurations. A detailed description can be found in Appendix A.2.

Fig. 8 shows the effect of assuming the wrong albedo value for the optimization. The reference orientation was calculated assuming an albedo for 0.2. Then the indicators (energy consumption, wasted energy and LCOH) were calculated using the optimal configuration but using a different albedo, which mean that these systems are suboptimal.

The LCOH of the double-sided system is the most resilent, followed by the single-sided LCOH, which has a positive impact (lower cost at higher albedo). The other indicators are underestimated if the albedo used has a lower value than the real one.

5.3. *Influence of non-ideal Faraday efficiency*

The system model assumed a Faraday efficiency of 1, which indicates that all the current is used for the generation of hydrogen. In reality, Faraday's efficiency depends on the applied current and the operating temperature [55]. A well-

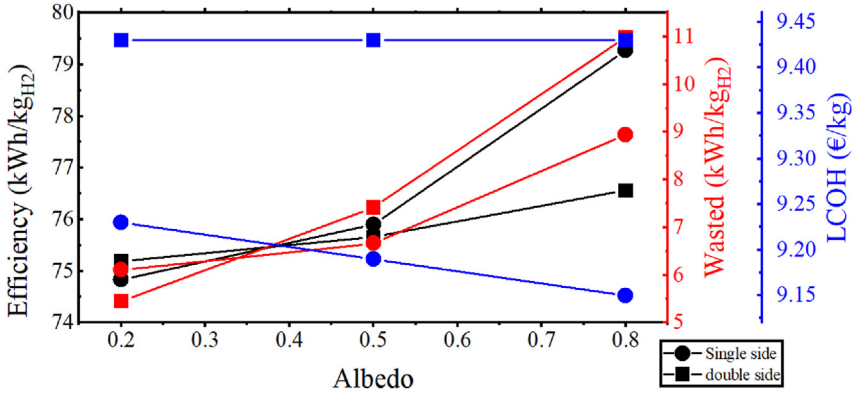

Fig. 8 – Effect of the albedo on the indicators. The reference system is optimized for an albedo of 0.2. Then the albedo was changed to 0.5 and 0.8 and the indicators calculated with the optimal system configuration but with these new albedo values. The system was not re-optimized for these values.

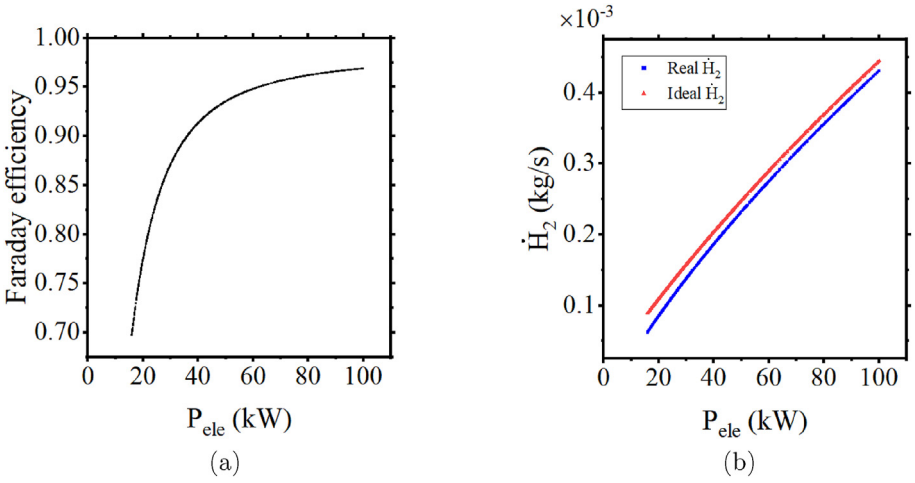

Fig. 9 – Influence of the Faraday efficiency on the hydrogen production. (a) Faraday efficiency with respect to the electrolyzer power, P_{ele}, and (b), a comparison of the ideal hydrogen flow ($\dot{H}_2$) as a function of the electrolyzer power, against the hydrogen flow when the Faraday efficiency is considered.

accepted model that describes the Faraday efficiency of an alkaline electrolyzer is Equation (27) [30].

$$\eta_F = \frac{i^2}{f_1 + i^2} f_2 \tag{27}$$

where the coefficients f_1 and f_2 are fitting parameters and are temperature dependent [30,55].

Fig. 9a shows that the Faraday efficiency is far from being constant and drops significantly at low electrolyzer powers. Fig. 9b shows that, with the ideal approach, the production of hydrogen per second (the hydrogen flow, $\dot{H}_2$) is overestimated.

This overestimation has an influence on the power that the compressor needs, which is proportional to the hydrogen flow as discussed in Section 2.2, Equation (11). When comparing the calculated compressor power under ideal conditions, to the power that the compressor would have needed if the Faraday efficiency was included, assuming that the power of the electrolyzer is the same, the median of the differences in the compressor power is only 0.44 kW, with a maximum of 0.77 kW. These differences are considerably small to influence the presented results and validate the assumption for a negligible influence of Faraday efficiency. This is critical because it facilitates the analytic calculation of the functions used in the Newton-Raphson method (Equations (21) and (23)).

An advantage of this methodology is that it is location-independent. The results presented in this work are based on data from The Netherlands. On locations with higher irradiance, the distribution of the GHI (Fig. 6a) is expected to have higher relative frequency values on higher irradiance bins. As a consequence, it is possible that the maximum operating limits of the electrolyzer are reached, leading to more wasted energy as a result of more energy being curtailed. With the observations from this study, it can be hypothesized that the oversize factors will be larger for sites with higher irradiance, as the orientation results will probably result in north-facing PV modules (for northern-hemisphere sites) to minimize the specific energy use and specific wasted energy. On the contrary, lower oversize factors are expected to lead to lower LCOH values.

This work considered ideal conditions for the PV system (flat ground, open space, uniform irradiance, constant albedo). Under realistic conditions, nearby obstacles change the irradiance seen by the module. The orientation results might change slightly for minimizing the LCOH, depending on the horizon profile. However, for specific energy use and wasted energy, they should not change significantly because the orientations are not harvesting all the incoming sunlight (vertical configurations or north-facing configurations).

6. Conclusions

This work presented the optimization of a stand-alone PV-electrolyzer system. The system consists of an alkaline electrolyzer and a compressor and is coupled using a DC-DC converter, which forces the PV system to operate always at its MPP. The optimum configuration was defined by three decision variables, namely, azimuth and tilt of the PV modules and the oversize factor. The optimum configuration to minimize energy use, wasted energy, and hydrogen cost, was found using the Particle Swarm Optimization algorithm.

Horizontally-placed modules are an interesting option for improving the usage of the PV system with only a small increase in the hydrogen cost.

The electrolyzer is best utilized in configurations that reduce the LCOH, because it operates more time at full load in comparison with configurations that minimize energy use or wasted energy. These last ones, prioritize longer operating times at very low loads, rather than operation at nominal power.

Although an idealized situation with Faraday's efficiency being 100% was considered, an analysis of a realistic situation when this efficiency is not ideal shows a slight overestimation of hydrogen production. This is translated into an increased

compressor power of less than 1 kW that can be considered negligible with respect to the power levels at hand in this work.

With the optimization procedure and analysis this work contributes to the needed efforts for the implementation of green hydrogen systems towards meeting the goals of the Net Zero Emissions scenarios of 2050.

Declaration of competing interest

The authors declare that they have no known competing financial interests or personal relationships that could have appeared to influence the work reported in this paper.

Acknowledgements

This activity is co-financed by Shell and a PPP-allowance from Top Consortia for Knowledge and Innovation (TKI's) of the Dutch Ministry of Economic Affairs and Climate in the context of the TU Delft e-Refinery program.

Appendix A. Supplementary data

Supplementary data to this article can be found online at https://doi.org/10.1016/j.ijhydene.2023.09.072.

REFERENCES

[1] IEA, Hydrogen. Tech. rep.. IEA; 2022.
[2] Tao M, Azzolini J, Stechel E, Ayers K, Valdez T. Review - engineering challenges in green hydrogen production systems. J Electrochem Soc 2022;169(5):54503.
[3] García-Valverde R, Espinosa N, Urbina A. Optimized method for photovoltaic-water electrolyser direct coupling. Int J Hydrogen Energy 2011;36:10574–86.
[4] Reuß M, Reul J, Grube T, Langemann M, Calnan S, Robinius M, Schlatmann R, Rau U. Solar hydrogen production: a bottom-up analysis of different photovoltaic-electrolysis pathways. Sustain Energy Fuels 2019;3:801–13.
[5] García-Valverde R, Miguel C, Martínez-Béjar R, Urbina A. Optimized photovoltaic generator-water electrolyser coupling through a controlled dc-dc converter. Int J Hydrogen Energy 2018;33:5352–62.
[6] Gallardo F, García J, Monforti Ferrario A, Comodi G, Chiu J. Assessing sizing optimality of off-grid ac-linked solar pv-pem systems for hydrogen production. Int J Hydrogen Energy 2022;47:27303–25.
[7] Atlam O, Barbir F, Bezmalinovic D. A method for optimal sizing of an electrolyzer directly connected to a pv module. Int J Hydrogen Energy 2011;36:7012–8.
[8] Mitra ED, Hlavacek WS. Parameter estimation and uncertainty quantification for systems biology models. Curr Opin Struct Biol 2019;18:9–18.
[9] Khalilnejad A, Abbaspour A, Sarwat A. Multi-level optimization approach for directly coupled photovoltaic-electrolyzer system. Int J Hydrogen Energy 2016;41:11884–94.
[10] Mas R, Berastain A, Antoniou A, Angeles L, Valencia S, Celis C. Genetic algorithms-based size optimization of directly coupled and indirectly coupled photovoltaic-electrolyzer systems. Energy Convers Manag 2022;270:116213.
[11] Maroufmashat A, Sayedin F, Khavas SS. An imperialist competitive algorithm approach for multi-objective optimization of direct coupling photovoltaic-electrolyzer systems. Int J Hydrogen Energy 2014;39(33):18743–57.
[12] Sayedin F, Maroufmashat A, Sattari S, Elkamel A, Fowler M. Optimization of photovoltaic electrolyzer hybrid systems; taking into account the effect of climate conditions. Energy Convers Manag 2016;118:438–49.
[13] Sayedin F, Maroufmashat A, Roshandel R, Khavas SS. Optimal design and operation of a photovoltaic–electrolyser system using particle swarm optimisation. Int J Sustain Energy 2016;35(6):566–82. https://doi.org/10.1080/14786451.2014.922974.
[14] Yang Z, Zhang G, Lin B. Performance evaluation and optimum analysis of a photovoltaic-driven electrolyzer system for hydrogen production. Int J Hydrogen Energy 2015;40:3170–9.
[15] Gillisen B, Heinrichs H, Stenzel P, Linssen L. Hybridization strategies of power-to-gas systems and battery storage using renewable energy. Int J Hydrogen Energy 2017;42:13554–67.
[16] Boudries R, Khellaf A, Aliane A, Ihaddaden L, Khida F. Pv system design for powering an industrial unit for hydrogen production. Int J Hydrogen Energy 2014;39(27):15188–95.
[17] Karacavus B, Aydin K. Hydrogen production and storage analysis of a system by using trnsys. J. Hydrog. Energy 2020;45:34608–19.
[18] Corengia M, Torres AI. Coupling time varying power sources to production of green-hydrogen: a superstructure based approach for technology selection and optimal design. Chem Eng Res Des 2022;183:235–49. https://doi.org/10.1016/j.cherd.2022.05.007.
[19] Pivetta D, Dall'Armi C, Taccani R. Multi-objective optimization of a hydrogen hub for the decarbonization of a port industrial area. J Mar Sci Eng 2022;10(2):231.
[20] Engstam L, Janke L, Sundberg C. Åke Nordberg, Grid-supported electrolytic hydrogen production: cost and climate impact using dynamic emission factors. Energy Convers Manag 2023;293:117458. https://doi.org/10.1016/j.enconman.2023.117458.
[21] Zhang S, Zhang N, Zhang X, Shi Q, Lu J, Dai H. Study on the optimization of system configuration of green hydrogen projects. In: 2022 7th international conference on power and renewable energy. ICPRE; 2022. p. 1260–3. https://doi.org/10.1109/ICPRE55555.2022.9960360.
[22] Yates J, Daiyan R, Patterson R, Egan R, Amal R, Ho-Baille A, Chang NL. Techno-economic analysis of hydrogen electrolysis from off-grid stand-alone photovoltaics incorporating uncertainty analysis. Cell reports Physical science 2020;1:100209. https://doi.org/10.1016/j.xcrp.2020.100209.
[23] Phan Van L, Hieu Hoang L, Nguyen Duc T. A comprehensive review of direct coupled photovoltaic-electrolyser system: sizing techniques, operating strategies, research progress, current challenges, and future recommendations. Int J Hydrogen Energy 2023. https://doi.org/10.1016/j.ijhydene.2023.03.257.
[24] Yang Z, Lin J, Zhang H, Lin B, Lin G. A new direct coupling method for photovoltaic module-pem electrolyzer stack for hydrogen production. Fuel Cell 2018;18(4):543–50. https://doi.org/10.1002/fuce.201700206.
[25] Su Z, Ding S, Gan Z, Yang X. Optimization and sensitivity analysis of a photovoltaic-electrolyser direct-coupling system in beijing. Int J Hydrogen Energy 2014;39(14):7202–15. https://doi.org/10.1016/j.ijhydene.2014.02.136.

[26] Laoun B, Khellaf A, Naceur MW, Kannan AM. Modeling of solar photovoltaic-polymer electrolyte membrane electrolyzer direct coupling for hydrogen generation. Int J Hydrogen Energy 2016;41(24):10120–35. https://doi.org/10.1016/j.ijhydene.2016.05.041.
[27] Paola A, Fabrizio Z, Fabio O. Techno-economic optimisation of hydrogen production by pv – electrolysis: "renhydrogen" simulation program. Int J Hydrogen Energy 2011;36(2):1371–81. https://doi.org/10.1016/j.ijhydene.2010.10.068.
[28] Mathworks. particleswarm - particle swarm optimization. 2022 [online].
[29] Miranda LJV, Moser A, Cronin SK, Carl -K, Jarcho A, Papadimitriou C, Nabé M, Erik, Speidell J, Bradahoward, Thomas. Pyswarms - a research toolkit for particle swarm optimization in python. 2017 [online].
[30] Ulleberg O. Modeling of advanced alkaline electrolyzers: a system simulation approach. Int J Hydrogen Energy 2003;28:21–33.
[31] Grigoriev SA, Fateev VN. Hydrogen production by water electrolysis. John Wiley & Sons, Ltd; 2017. p. 231–76. Ch. 6.
[32] Harrison K, Levene JI. Electrolysis of water. Springer-Verlag; 2008. p. 41–63. Ch. 3.
[33] Abderezzak B. 2 - charge transfer phenomena. In: Abderezzak B, editor. Introduction to transfer phenomena in PEM fuel cell. Elsevier; 2018. p. 53–83. https://doi.org/10.1016/B978-1-78548-291-5.50002-0.
[34] Fragiacomo P, Genovese M. Modeling and energy demand analysis of a scalable green hydrogen production system. Int J Hydrogen Energy 2019;44:30237–55.
[35] Moran M, Shapiro H. Fundamentals of engineering Thermodynamics. Wiley; 2006.
[36] Connor N. What is isentropic process - definition. 2019 [online].
[37] Hall N, editor. Isentropic compression; 2021 (or expansion) [online].
[38] Knap W. Basic measurements of radiation at station Cabauw (2013-01). PANGAEA; 2013. https://doi.org/10.1594/PANGAEA.807193.
[39] Smets A, Jäger K, Isabella O, van Swaaij R, Zeman M. Solar energy: the physics and engineering of photovoltaic conversion, technologies and systems. UIT Cambridge; 2016.
[40] Stultz JW. Thermal and other tests of photovoltaic modules performed in natural sunlight. J Energy 1979;3(6):363–72. https://doi.org/10.2514/3.62445.
[41] TrinaSolar. The tallmax m framed 144 layout module. 2019 (datasheet) [online].
[42] Alam M, Kumar K, Verma S, Dutta V. Renewable sources based dc microgrid using hydrogen energy storage: modeling and experimental analysis. Sustain Energy Technol Assessments 2020;42:100840.
[43] Kennedy J, Eberhart R. Particle swarm optimization. In: Proceedings of ICNN'95 - international conference on neural networks, vol. 4; 1995. p. 1942–8. vol. 4.
[44] Slowik A, Kwasnicka H. Nature inspired methods and their industry applications - swarm intelligence algorithms. IEEE Trans Ind Inf 2018;14(3):1004–15.
[45] Sayedin F, Maroufmashat A, Al-Adwani S, Khavas SS, Elkamel A, Fowler M. Evolutionary optimization approaches for direct coupling photovoltaic-electrolyzer systems. In: 2015 international conference on industrial engineering and operations management. IEOM; 2015. p. 1–8. https://doi.org/10.1109/IEOM.2015.7093884.
[46] Fuel Cells and Hydrogen Obervatory. Levelized cost of hydrogen. 2022 [online].
[47] Rezaei M, Akimov A, Gray EM. Economics of solar-based hydrogen production: sensitivity to financial and technical factors. Int J Hydrogen Energy 2022;47(65):27930–43. https://doi.org/10.1016/j.ijhydene.2022.06.116.
[48] TRACTEBEL Engineering, Hinicio. Study on early business cases for h2 in energy storage and more broadly power to h2 applications, Tech. rep. Fuel Cells and Hydrogen Joint Undertaking 2017.
[49] Mraoui A, Khellaf A. Optimization of the design of hydrogen production systems based on product cost. J Sol Energy Eng 2020;142:41003.
[50] Al-Buraiki AS, Al-Sharafi A. Hydrogen production via using excess electric energy of an off-grid hybrid solar/wind system based on a novel performance indicator. Energy Convers Manag 2022;254:115270. https://doi.org/10.1016/j.enconman.2022.115270.
[51] Murphy FH, Sen S, Soyster AL. Electric utility capacity expansion planning with uncertain load forecasts. IIE Trans 1982;14:52–9.
[52] Taibi E, Blanco H, Miranda R, Carmo M. Green hydrogen cost reduction. scaling up electrolyzers to meet the 1.5°c climate goal, Tech. rep.. IRENA; 2020.
[53] Uchman W, Kotowicz J. Varying load distribution impacts on the operation of a hydrogen plant. Int J Hydrogen Energy 2021;46:39095–107.
[54] Efron B. The jacknife, the bootstrap, and other resampling plans. philadelfie, USA: Society for Industrial and applied mathematics; 1982.
[55] Hernández-Gómez A, Ramirez V, Guilbert D. Investigation of pem electrolyzer modeling: electrical domain, efficiency, and specific energy consumption. Int J Hydrogen Energy 2020;45:14625–39.